Simulation of a Three-Step One-Column Pressure Swing Adsorption Process

Z. P. Lu, J. M. Loureiro, and A. E. Rodrigues
Lab. of Separation and Reaction Engineering, School of Engineering, University of Porto, 4099 Porto Codex, Portugal

M. D. LeVan
Dept. of Chemical Engineering, University of Virginia, Charlottesville, VA 22903

Separation of a binary mixture by a three-step one-column pressure swing adsorption process in isothermal and adiabatic cases has been studied. The separation performance of the process is characterized by three parameters: enrichment, recovery and productivity. It has been compared at various operating conditions. The evolution of the bed performance from cycle to cycle and the bed dynamics at cyclic steady state have also been addressed.

Introduction

Pressure swing adsorption (PSA) is a modern separation process based on the effect of pressure and cycle conditions on adsorption equilibrium and rate behavior. Applications include the production of oxygen and nitrogen from air, hydrogen purification, air drying, methane/carbon dioxide separation, and helium recovery.

A wide variety of PSA cycles have been established. The traditional and often analyzed Skarstrom cycle has four steps: pressurization, adsorption, blowdown, and purge. In recent years, many variations have been made on this cycle. Some rather complicated multistep cycles are currently used industrially involving many beds with pressure equilibration steps and pressurization and blowdown flows in both directions. Similarly, there has been considerable interest and commercial activity in simple cycles with fewer than four steps.

The one-column, rapid pressure swing adsorption (RPSA) process was invented by Kadlec and coworkers (1971, 1972) for the separation of a nitrogen and methane mixture. It consists of two steps with equal time lengths: pressurization/feed followed by exhaust (blowdown). Substantial refinement of this process was made by Jones and Keller (1981) for commercial oxygen production from air. Compared with the normal PSA process, a much higher adsorbent productivity is obtained in the process (Yang, 1987). The dynamics of this process are very complex due to the existence of short cycle times and large pressure gradients in the bed.

While modeling of PSA processes has been reasonably extensive for the Skarstrom cycle and a few variations, few models have been published concerning the complicated multibed cycles or the simple cycles with complex dynamics. Concerning simple cycles, a well-stirred cell local equilibrium model has been used by Fernandez and Kenney (1983) to describe the three-step one-column PSA separation of air on a molecular sieve adsorbent, and agreement of the model with experiments was found for long cycle times. Cheng and Hill (1985) developed a modified well-stirred cell local equilibrium model, which includes effects of the unpacked "dead volumes" at the column ends, to simulate the separation performance of a helium and methane mixture by the three-step one-column process. The authors stated that the discrepancy of the model prediction and experimental results was due to the omission of flow resistance and heat release.

A variety of contributions, relevant to our purposes, have been made to the modeling of PSA processes. The local equilibrium model is widely used to get a useful insight into the problems in PSA separations (Knaebel and Hill, 1985; Kayser and Knaebel, 1986, 1989; Suh and Wankat, 1989a,b); however, in these works the pressure drop and the temperature fluctuation are assumed to be negligible. Recently, the importance of pressure gradients in the bed during pressurization and blowdown steps in PSA process has been assessed, and dynamic analyses of these steps have been made (Yang and Doong, 1988; Sundaram and Wankat, 1988; Hart et al., 1990; Rodrigues et al., 1991a,b; Scott, 1991; Lu et al., 1992a). Also the temperature variations in PSA processes have been recognized in several studies (Yang and Cen, 1986, Kumar, 1989; Lu et al., 1992b).

Correspondence concerning this article should be addressed to A. E. Rodrigues.

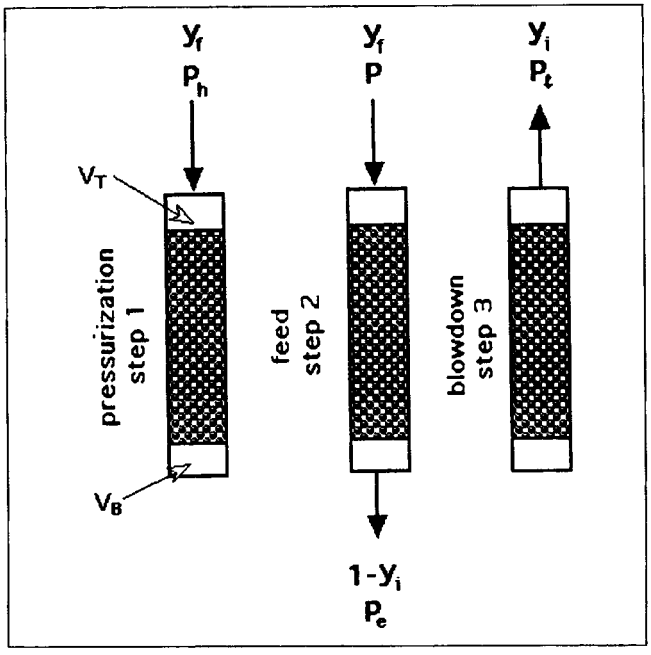

Figure 1. Sketch of the three-step one-column PSA process.

This article contributes to the modeling of simple PSA cycles with complex dynamics. We develop a collocation-based mathematical model for the three step, one column cycle of Cheng and Hill (1985) and then use the model to perform parametric studies. Specifically, we address the following problems concerning the dynamics of the process: (i) the separation performance under various operating conditions; (ii) the evolution of the process from different initial bed conditions to the cyclic steady state; and (iii) the bed dynamics of the process at the cyclic steady state. Our model is of the local equilibrium type and includes a momentum balance, making the model especially appropriate for analyzing processes with small particles for which the pressure drop in the bed can be large. We study the effects of isotherm capacity and nonlinearity, incomplete pressurization and blowdown, dead volumes at the ends of the column, feed composition, and isothermal and adiabatic operation.

Process Description

The process modeled is a three-step one-column process, shown in Figure 1, used by Cheng and Hill (1985). The mixture to be separated consists of one inert and one adsorbable species. The cycle of the process is composed of pressurization from low pressure to high pressure with feed, feed at high pressure with withdraw of a light product (inert) from the product end and blowdown of the column to low pressure. Inert enriched gas is obtained as a product at high pressure during the feed step, and an enriched stream of the adsorbable species is obtained during the blowdown step. "Dead" volumes exist at both sides of the packed adsorbents and behave as CSTRs. The pressurization and blowdown rates of the column to high and low pressure respectively are controlled by valves.

Mathematical Model

The local equilibrium model is used to simulate the three-step one-column PSA separation of a binary mixture (one adsorbable species i, and one inert (light) species) that is, no intraparticle and film mass-transfer and heat-transfer resistances are assumed. Additional assumptions are:

- The flow pattern can be described by axial dispersed plug flow.
- The superficial velocity inside the bed follows Ergun's law locally.
- Ideal gas behavior; the temperature dependence of gas and solid thermodynamic properties is assumed to be negligible.
- Adsorption equilibrium equations are described by a linear isotherm or a Langmuir isotherm ($q_i = q_m k c y_i / 1 + k c y_i$); the equilibrium constant shows the normal exponential temperature dependence, that is, $k \propto e^{-\Delta H/RT}$.

Introducing the dimensionless variables:

$$f=\frac{c}{c_o},\ u^*=\frac{u}{u_o},\ \tilde{T}=\frac{T}{T_{oo}},\ P^*=\tilde{T}f=\frac{P}{P_o},\ x=\frac{z}{L},\ \theta=\frac{t}{\tau_o},\ \tau_o=\frac{\epsilon L}{u_o}$$

The dimensionless model equations can be written (Lu et al., 1992b):

Mass balance for species i:

$$\frac{\partial}{\partial x}\left(\frac{u^* f}{Pe_m}\frac{\partial y_i}{\partial x}\right)-\frac{\partial (u^* f y_i)}{\partial x}$$
$$=\frac{\epsilon_t}{\epsilon}\left\{\frac{\partial (f y_i)}{\partial \theta}+\frac{\epsilon_r k' q^*}{[1+(k'-1)\Phi f y_i]^2}\left[\frac{\partial (f y_i)}{\partial \theta}-\frac{\beta_h}{\beta_r}\frac{f y_i}{\tilde{T}^2}\frac{\partial \tilde{T}}{\partial \theta}\right]\right\} \quad (1)$$

Overall mass balance:

$$-\frac{\partial (u^* f)}{\partial x}$$
$$=\frac{\epsilon_t}{\epsilon}\left\{\frac{\partial f}{\partial \theta}+\frac{\epsilon_r k' q^*}{[1+(k'-1)\Phi f y_i]^2}\left[\frac{\partial (f y_i)}{\partial \theta}-\frac{\beta_h}{\beta_r}\frac{f y_i}{\tilde{T}^2}\frac{\partial \tilde{T}}{\partial \theta}\right]\right\} \quad (2)$$

Energy balance:

$$\frac{\partial}{\partial x}\left(\frac{u^*}{Pe_h}\frac{\partial \tilde{T}}{\partial x}\right)-u^* f\frac{\partial \tilde{T}}{\partial x}$$
$$=\frac{\epsilon_t}{\epsilon}\left\{-\beta_r \tilde{T}\frac{\partial f}{\partial \theta}+[f(1-\beta_r)+\epsilon_r\beta_c]\frac{\partial \tilde{T}}{\partial \theta}-\frac{\epsilon_r\beta_h k' q^*}{[1+(k'-1)\Phi f y_i]^2}\right.$$
$$\left.\times\left[\frac{\partial (f y_i)}{\partial \theta}-\frac{\beta_h}{\beta_r}\frac{f y_i}{\tilde{T}^2}\frac{\partial \tilde{T}}{\partial \theta}\right]\right\}+\alpha_{hw}(\tilde{T}-\tilde{T}_w) \quad (3)$$

where $\Phi = c_o/c_h$ and $\epsilon_r = \frac{(1-\epsilon)(1-\epsilon_p)}{\epsilon_t}$.

Momentum equation:

$$-\left(f\frac{\partial \tilde{T}}{\partial x}+\tilde{T}\frac{\partial f}{\partial x}\right)=b_4 u^*+b_5 f(u^*)^2 \quad (4)$$

$$b_4=\frac{150\mu(1-\epsilon)^2L}{d_p^2\epsilon^3P_o}u_o;\ b_5=\frac{1.75\rho_{go}(1-\epsilon)L}{P_od_p\epsilon^3}u_o^2 \quad (4a)$$

where

$$\frac{1}{Pe_m}=\frac{\epsilon D_{ax}}{Lu}=\frac{b_1(\tilde{T})^{1/2}}{u^*f}+b_2 \quad (5)$$

$$b_1=\frac{\epsilon\gamma_1 D_{mo}}{Lu_o};\ b_2=\frac{\epsilon\gamma_2 d_p}{L} \quad (5a)$$

$$\frac{1}{Pe_h}=\frac{k_{hx}}{c_oc_{pg}uL}=\frac{b_3}{u^*}+b_4f \quad (6)$$

$$b_3=\frac{\gamma_1' k_{hg}}{c_oc_{pg}Lu_o};\ b_4=\frac{\gamma_2' d_p}{L} \quad (6a)$$

$$q^*=\frac{q_mk}{1+kc_h};\ k'=1+kc_h \quad (7)$$

$$\beta_h=\frac{-\Delta H}{c_{pg}T_{oo}};\ \beta_r=\mathrm{R}/c_{pg};\ \beta_c=\frac{\rho_sc_{ps}}{c_oc_{pg}} \quad (8)$$

$$\alpha_{hw}=\frac{4h_w}{\epsilon Dc_{pg}c_o}\tau_o \quad (9)$$

When $\alpha_{hw}=0$, the system is adiabatic; when $\beta_c\to\infty$, the system reduces to the isothermal case, $\partial\tilde{T}/\partial x$ and $\partial\tilde{T}/\partial\theta$ are equal to zero and Eq. 7 reduces to:

$$q_o^*=\frac{q_mk_o}{1+k_oc_h};\ k_o'=1+k_oc_h \quad (10)$$

It should be noted that for porous particles γ_1 and γ_2 usually take values of 20 and 0.5, respectively (Ruthven, 1984), and γ_1' is a function of the heat conductivity ratio between the particle and the fluid in a packed bed. It equals to eight in this article, and γ_2' is about 0.5 (Wakao and Chen, 1983).

The PSA cycle usually starts with the pressurization step. Two initial conditions, feed-saturated and clean bed, are used in the simulation. These are:

$$\theta=0,\ y_i=y_f;\ \tilde{T}=\tilde{T}_o=1;\ P^*=P_l^*;\ 0<x\le 1 \quad (11)$$

and

$$\theta=0,\ y_i=0;\ \tilde{T}=\tilde{T}_o=1;\ P^*=P_l^*;\ 0<x\le 1 \quad (11a)$$

Boundary conditions on the bulk fluid in the bed for cyclic operation are:

(a) pressurization

$$x=0,\ \tilde{T}f=(P_h^*-P_l^*)[1-\exp(-M_p\theta)]+P_l^*;$$

$$-\frac{1}{Pe_m}\frac{\partial y_i}{\partial x}+y_i=y_f;\ -\frac{1}{Pe_h}\frac{\partial\tilde{T}}{\partial x}+\tilde{T}=\tilde{T}_f \quad (12)$$

$$x=1,\ \frac{\partial f}{\partial x}=0;\ \frac{\partial y_i}{\partial x}=0;\ \frac{\partial\tilde{T}}{\partial x}=0 \quad (13)$$

(b) feed

$$x=0,\ u^*P^*=u_r^*P_h^*;\ -\frac{1}{Pe_m}\frac{\partial y_i}{\partial x}+y_i=y_f;\ -\frac{1}{Pe_h}\frac{\partial\tilde{T}}{\partial x}+\tilde{T}=\tilde{T}_f$$

$$x=1,\ \tilde{T}f=P_e^*;\ \frac{\partial y_i}{\partial x}=0;\ \frac{\partial\tilde{T}}{\partial x}=0 \quad (14)$$

(c) blowdown

$$x=0,\ \tilde{T}f=(P_l^*-P_h^*)[1-\exp(-M_b\theta)]+P_h^*;$$

$$\frac{\partial y_i}{\partial x}=0;\ \frac{\partial\tilde{T}}{\partial x}=0 \quad (15)$$

at $x=1$ the conditions are the same as Eq. 13.

where parameters M_p and M_b are fixed by the pressurization and blowdown valve coefficients.

"Dead" Volumes

In the packed fixed-bed, usually the "dead" volumes at both sides of the packing are difficult to avoid. Sometimes they strongly affect the bed behavior. In the three-step one-column PSA process, the "dead" volume at the feed end was considered to decrease the separation performance, in contrast with the "dead" volume at the product end (Cheng and Hill, 1985). The hydrodynamics in the "dead" volume is very similar to that in the continuous stirred tank reactor (CSTR); for the isothermal case mass balances in the "dead" volumes in the feed and product ends of the column can be written as (Ramkrishna and Amundson, 1974):

In the top (feed) end "dead" volume:

- pressurization

$$\frac{\partial f}{\partial\theta}=\frac{1}{\beta_T}(u_p^*f_h-u^*f) \quad (16)$$

$$\frac{\partial y_i}{\partial\theta}=\frac{u_p^*f_h}{f\beta_T}(y_f-y_i)+\frac{u^*}{\beta_TPe_m}\frac{\partial y_i}{\partial x} \quad (17)$$

- feed

$$\frac{\partial f}{\partial\theta}=\frac{1}{\beta_T}(u_r^*f_h-u^*f) \quad (18)$$

$$\frac{\partial y_i}{\partial\theta}=\frac{u_r^*f_h}{f\beta_T}(y_f-y_i)+\frac{u^*}{\beta_TPe_m}\frac{\partial y_i}{\partial x} \quad (19)$$

- blowdown

$$f=(f_l-f_h)[1-\exp(-M_b\theta)]+f_h \quad (20)$$

$$\frac{\partial y_T}{\partial\theta}=\frac{u^*}{\beta_T}(y_T-y_i)+\frac{u^*}{\beta_TPe_m}\frac{\partial y_i}{\partial x} \quad (21)$$

In the bottom (product) end "dead" volume:

- pressurization

$$\frac{\partial f}{\partial \theta}=\frac{u^* f}{\beta_B} \tag{22}$$

$$\frac{\partial y_B}{\partial \theta}=\frac{u^*}{\beta_B}(y_i-y_B)-\frac{u^*}{\beta_B Pe_m}\frac{\partial y_i}{\partial x} \tag{23}$$

- feed

$$f=(f_e-f_h)[1-\exp(-M_f\theta)]+f_h \tag{24}$$

$$\frac{\partial y_B}{\partial \theta}=\frac{u^*}{\beta_B}(y_i-y_B)-\frac{u^*}{\beta_B Pe_m}\frac{\partial y_i}{\partial x} \tag{25}$$

- blowdown

$$\frac{\partial f}{\partial \theta}=\frac{u^* f}{\beta_B} \tag{26}$$

$$y_i-\frac{1}{Pe_m}\frac{\partial y_i}{\partial x}=y_B \tag{27}$$

where $\beta_T=V_T/\epsilon AL$ and $\beta_B=V_B/\epsilon AL$, V_T and V_B are the "dead" volumes at feed and product ends, respectively.

The initial conditions of each step are the final values of the previous step.

Process Performance

The process performance under cyclic steady state can be described by the following parameters:

(a) the average enrichment of the light component in the product stream

$$\mathrm{EN}=\frac{1-\bar{y}_p}{1-y_f} \tag{28}$$

where $\bar{y}_p$ is the average mole fraction of the adsorbable species in the product stream, given by:

$$\bar{y}_p=\frac{\int_0^{\theta_f}(u^* f y_i)_{x=1}d\theta}{\int_0^{\theta_f}(u^* f)_{x=1}d\theta} \tag{29}$$

(b) the dimensionless productivity N_{prod}, normalized by the reference mole flux $u_o c_o$

$$N_{\mathrm{prod}}=\frac{1}{\theta_t}\int_0^{\theta_f}(u^* f)_{x=1}d\theta \tag{30}$$

where $\theta_t=\theta_p+\theta_f+\theta_b$, and θ_t, θ_p, θ_f and θ_b are total cycle, pressurization, feed and blowdown times, respectively.

(c) the recovery of the light component in the product stream

$$\mathrm{RE}=\mathrm{EN}\times\mathrm{CUT} \tag{31}$$

Table 1. Parameter Values Used in the Simulations of PSA Cycle

$P_h=5.00$ bar	$-\Delta H=5{,}000$ cal/mol·K
$P_l=1.00$ bar	$c_{ps}=0.25$ cal/g of solid K
$P_e=4.5$ and 4.0 bar	$c_{pg}=7.68$ cal/mol·K
L = 100 cm	$k_{hg}=5\times10^{-5}$ cal/cm·s·K
$\epsilon=0.43$	$\mu=10^{-4}$ g/s·cm
$\epsilon_p=0.595$	$P_o=1$ bar
$\rho_s=2.1$ g/cm^3	$T_{oo}=298$ K
$d_p=0.03$ cm	$c_o=4.464\times10^{-4}$mol/cm^3
$\rho_{go}=10^{-3}$ g/cm^3	$u_o=92$ cm/s
$D_{mo}=0.625$ cm^2/s	$u_r=34.8$ cm/s
$y_f=0.25, 0.5, 0.75$	$\tau_o=0.467$ s
$\gamma_1=20$; $\gamma_2=0.5$	$\beta_c=1{,}573$
$\gamma_1'=8$; $\gamma_2'=0.5$	$M_p=20$; $M_b=20$
$k_o'=1, 2, 6$	$\beta_T=\beta_B=0, 0.1, 0.25$
$q_0^*=10, 20, 60$	

where the product cut (CUT) is given by

$$\mathrm{CUT}=\frac{N_{\mathrm{prod}}}{N_p+N_f} \tag{32}$$

with

$$N_p+N_f=\frac{1}{\theta_t}\left[\int_0^{\theta_p}(u^* f)_{x=0}d\theta+\int_0^{\theta_f}(u^* f)_{x=0}d\theta\right] \tag{33}$$

The dimensionless pressurization and feed rates, normalized by the reference mole flux, are N_p and N_f, respectively.

Simulation Results and Discussion

Model equations were solved with the PDECOL package. Normally, 15 elements were used in the axial direction unless noted. The first-order ordinary equations in the "dead" volumes were solved by the Runge-Kutta method. The computational CPU times for one cycle under cyclic steady state (three-step) was around 10–20 s on an IBM RS/6000-530 computer. Numerical oscillations in axial mole fraction profiles in the upstream region were found in simulations since there Peclet numbers are high, as we have noticed before (Lu et al, 1992, 1993). Therefore, different numbers of finite elements in the bed were tested; almost no oscillations were found when the number of finite elements is 100. However, the relations between the process parameters do not change whatever the number of finite elements is used. The values used in the simulations are listed in Table 1 and were taken from the works of Cen and Yang (1986) and Yang and Cen (1986).

Performance is only related to the pressurization and blowdown amounts, and it is not affected by the pressurization and blowdown rates (Rodrigues et al., 1992a), that is, cycle times. So, we think that this criterion is a reasonable choice. The pressurization time θ_p is based on $|f\tilde{T}(x=1)-P_h^*|/P_h^*=\mathrm{PE}\%$ and θ_b blowdown time is based on $|f\tilde{T}(x=1)-P_l^*|/P_l^*=\mathrm{BE}\%$. In the three-step one-column PSA process studied in this article, the separation performance (enrichment-cut relation) is not related to the cycle time (Cheng and Hill, 1985; Rodrigues et al., 1992a), and it is almost linear in the reasonable operating region when local equilibrium dominates the process (Rodrigues et al., 1992a). High adsorbent productivity can be

obtained depending on the equipment capability and when mass transport resistance starts to be important. As pointed by Jones and Keller (1981), the optimum bed design and operating conditions occur just where mass-transfer resistance begin to be significant. For this reason, we will use different ways to determine the step times for different objectives as discussed below.

Separation performance under various operating conditions

In this section, we use the pressure at the closed end of the bed in pressurization and blowdown to determine the times for pressurization and blowdown steps. The feed time θ_f is based on the reference feed velocity for a given product cut, that is, $u^*\theta_f$ is constant.

The simulation calculations were carried out to understand how the separation performance is affected by: (a) the nature of the adsorption isotherm, $k_o' = 1$, 2, 6 and $q_o^* = 10$, 20, 60; (b) the feed composition, $y_f = 0.25$, 0.5, 0.75; (c) incomplete pressurization, PE = 0.1, 5, 20; and incomplete blowdown, BE = 0.05, 10, 50; (d) the "dead" volumes, β_B, $\beta_T = 0$, 0.1, 0.25; (e) the temperature variations: adiabatic and isothermal.

The simulation results reported here by using the equilibrium model are based on complete pressurization and blowdown, that is, PE < 0.1 and BE < 0.5, except in the cases where incomplete pressurization and blowdown were considered. The base case treated here is: $q_o^* = 20$, $k_o' = 2$ and $y_f = 0.5$. If it is not stated otherwise, the isothermal case is presented. We will discuss below how the separation performance is influenced by several factors.

Effect of the equilibrium isotherm. The adsorption isotherm used in the article is the Langmuir isotherm for $k_o' > 1$. When $k_o' \to 1$ the Langmuir isotherm reduces to the linear isotherm with slope q_o^*. It should be noted that $k_o' = 1$ means $k_o c_h << 1$. The effects of the nature of the isotherm and adsorption capacities on separation performance are shown in Figures 2a and 2b, respectively. The enrichment-recovery relation is strongly dependent of the q_o^* value; however, its shape is almost the same for the different q_o^* values. The parameter k_o' of the isotherm does not affect the separation performance much. The Langmuir adsorption isotherm is favorable in adsorption (pressurization and feed steps) but unfavorable in desorption (blowdown, Lu et al., 1992), so the total effect of k_o' is not great as shown in Figure 2a. For higher adsorption capacity, the treated amount of gas mixture for a given amount of adsorbent is larger; therefore a higher amount of the adsorbable species is adsorbed in the adsorption steps and more concentrated adsorbable species is obtained in the blowdown step (Lu et al., 1992); so, the separation performance is improved.

Incomplete pressurization and blowdown. Particle size, pressurization, feed and blowdown rates do not significantly affect the separation performance predicted by the equilibrium model (Rodrigues et al., 1992a). However, it is influenced by incomplete pressurization and blowdown steps. By "incomplete" we mean that the pressure at the closed end of the bed does not reach the imposed pressure at the open end of the bed, that is, pressure profiles inside the bed at the end of the pressure changing steps are not flat. The effect of PE and BE on the separation performance is shown in Figures 3a and 3b, respectively. Except at low product recovery, incomplete pressurization almost does not significantly affect the separation performance. However, incomplete blowdown affects the enrichment-recovery relation when BE is larger than 10. This is why Jones and Keller (1981) suggested the use of a long exhaust step. In this three-step PSA process, the purge of the adsorbable species is combined with the blowdown. Incomplete blowdown reduces the function of purge, so the separation performance is reduced.

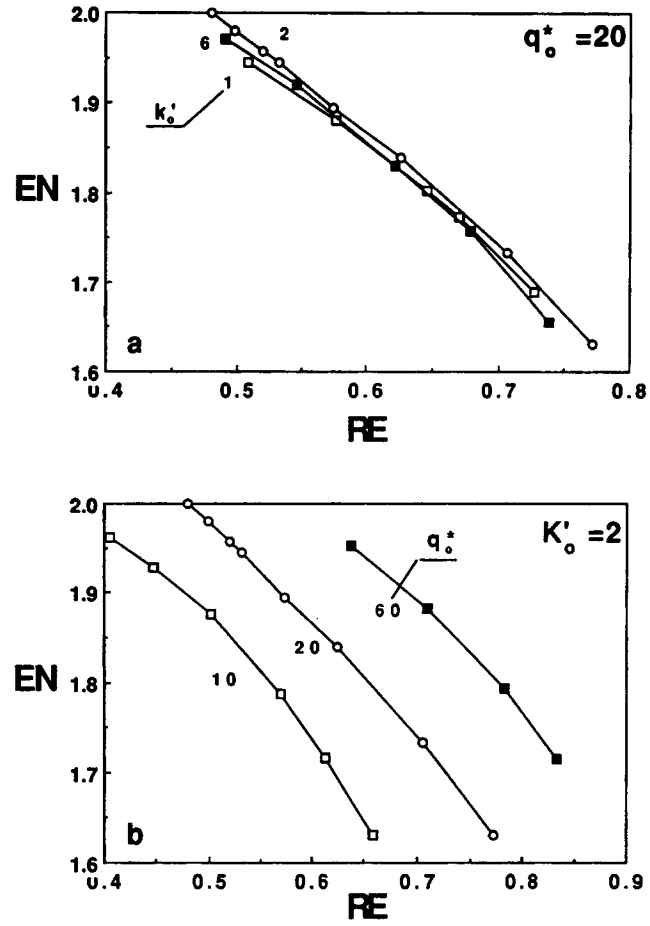

Figure 2. Effect of the adsorption isotherms on enrichment-recovery (EN-RE) relation.

(a) Effect of the nature of the adsorption isotherms; (b) effect of the adsorption capacity.

"Dead volumes" and feed composition. The presence of "dead volumes" at both ends of the bed is difficult to avoid. Sometimes, they strongly influence the bed behavior. For the system reported here, the bottom dead volume seems to improve the separation performance; however, the top dead volume decreases it, and the total effect seems to be marginal (Cheng and Hill, 1985). Figure 4 shows the enrichment-recovery relation for different values of the top and bottom "dead volume." The bottom "dead volume" leads to a small improvement on separation only for high recovery. The top "dead volume" seems to dominate the effect of the dead volumes, and it results in an obvious decrease in the enrichment for a given recovery, particularly at small recovery. Except in Figure 4, the "dead volumes" were not taken into account in simulations.

The average light species concentration in the product as a

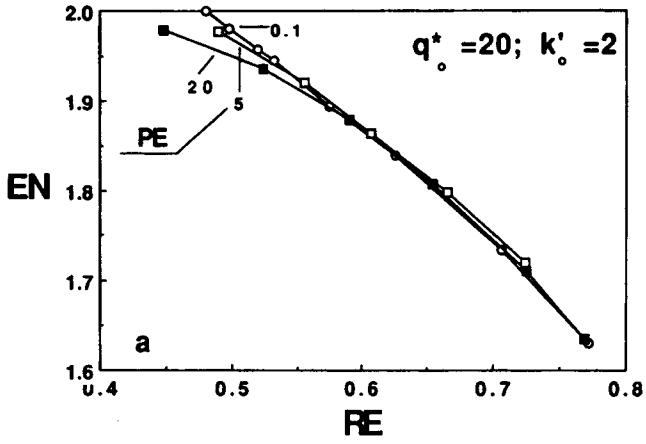

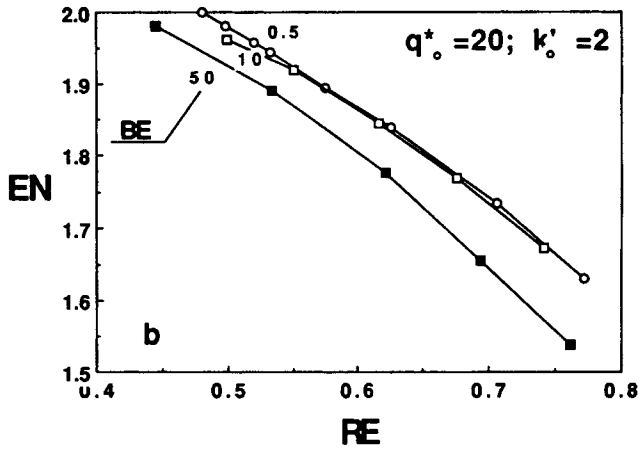

Figure 3. Effect of the incomplete pressurization (a) and incomplete blowdown (b) on enrichment-recovery relation.

function of recovery for different feed compositions is shown in Figure 5. The separation performance is much worse for higher mole fractions of the adsorbable species in the feed. All cases treated above are for the isothermal case.

Isothermal and adiabatic cases. The temperature variation during adsorption and desorption in bulk separation always

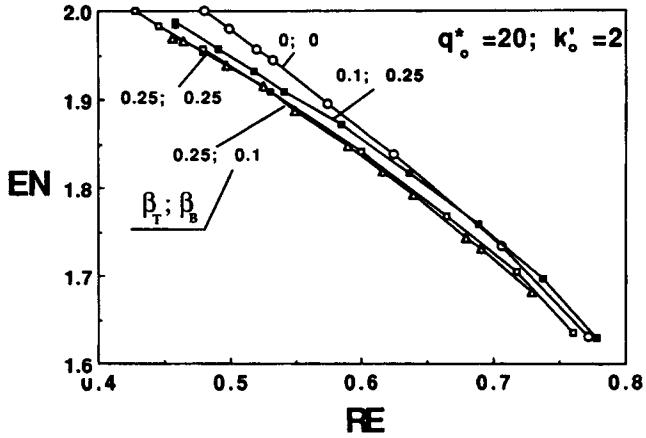

Figure 4. Effect of the "dead" volumes on enrichment-recovery relation.

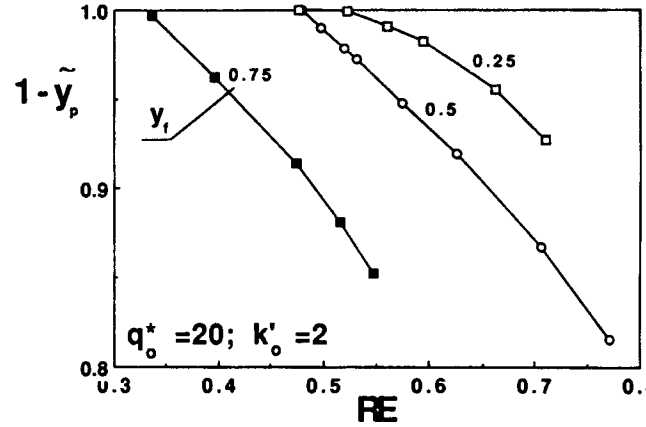

Figure 5. Average mole fraction of the light species in product as a function of recovery for various feed composition.

decreases the separation performance (Cen and Yang, 1986; Lu et al., 1992; Rodrigues et al., 1992a). Comparison between the isothermal case (full lines) and adiabatic cases (dashed lines) is presented in Figure 6. The shapes of EN-RE relation for the isothermal case and the adiabatic case are similar, and the differences of the enrichment for a given recovery between the isothermal and the adiabatic cases for different adsorption capacities almost does not change. If the heat transport through the column wall is considered or high heat-capacity adsorbent is used (Yang and Cen, 1986; Lu et al., 1992), the separation performance should be somewhere between the isothermal and adiabatic limits.

The enrichment-cut relation (EN-CUT) is almost linear in the region of interest, so the enrichment-recovery (EN-RE) curve is concave, when the interphase equilibrium dominates, that is, the equilibrium model is used. This is because the concentration front of the adsorbable species during the production or feed step is always sharp and, at higher product cut, the concentration profile penetrates deeper in the bed (Rodrigues et al., 1991a). However, the enrichment-productivity relation (EN-N_{prod}) has a convex shape for the equilibrium model, as shown by Rodrigues et al. (1992b). The number

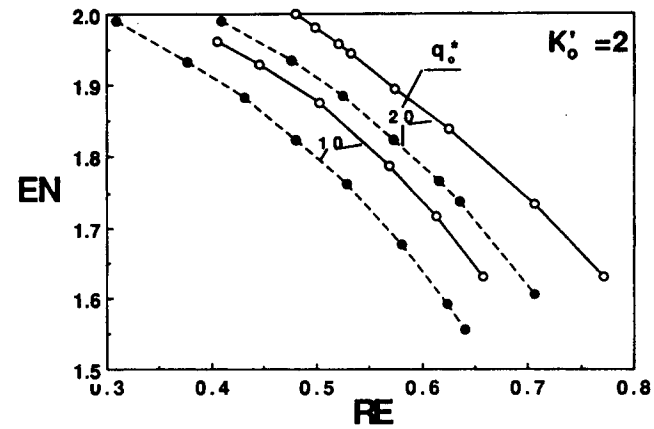

Figure 6. Enrichment of the light species as a function of recovery for different adsorption capacity in isothermal (full lines) and adiabatic (dashed lines) cases.

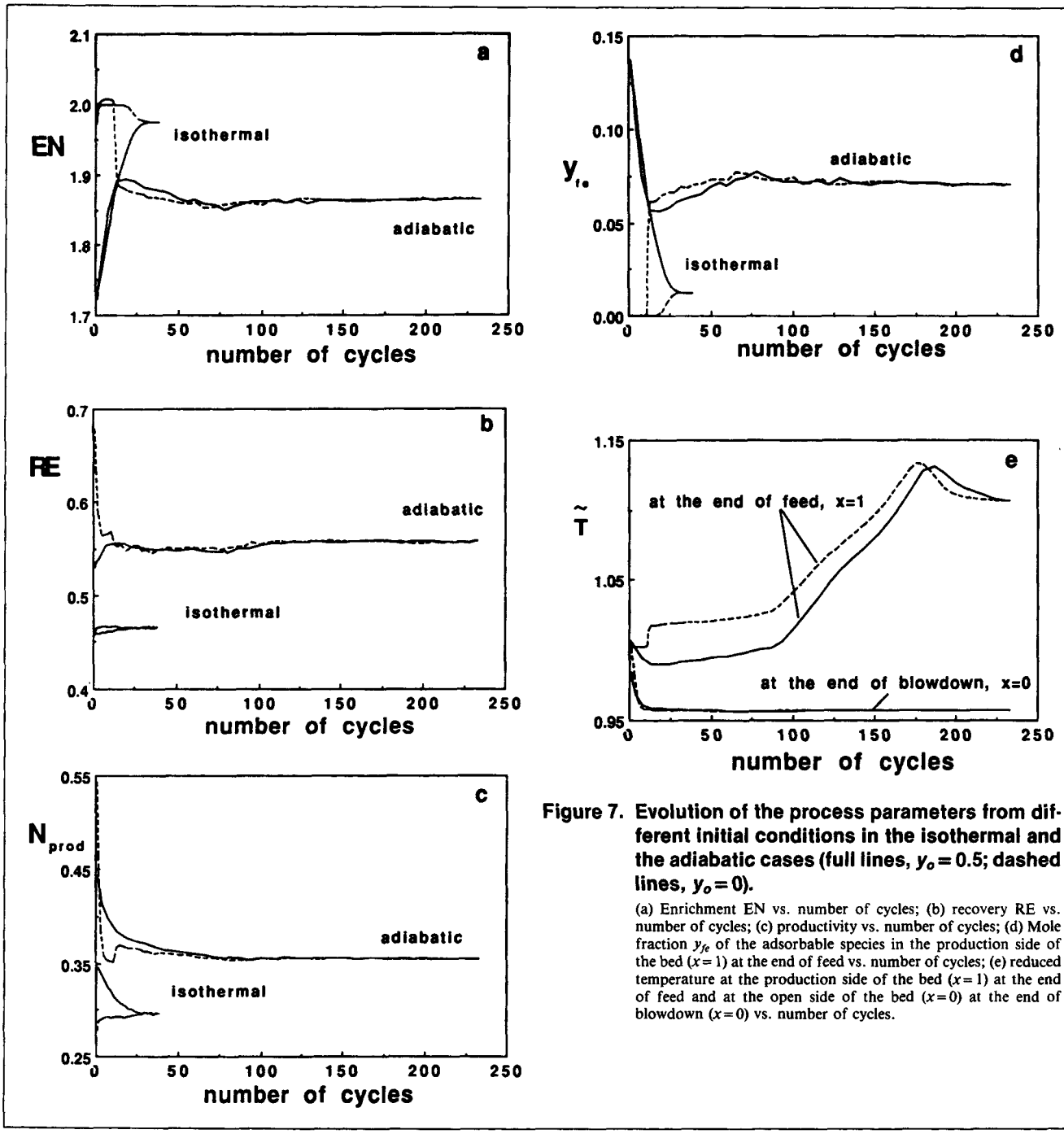

Figure 7. Evolution of the process parameters from different initial conditions in the isothermal and the adiabatic cases (full lines, $y_o = 0.5$; dashed lines, $y_o = 0$).

(a) Enrichment EN vs. number of cycles; (b) recovery RE vs. number of cycles; (c) productivity vs. number of cycles; (d) Mole fraction y_{fe} of the adsorbable species in the production side of the bed ($x = 1$) at the end of feed vs. number of cycles; (e) reduced temperature at the production side of the bed ($x = 1$) at the end of feed and at the open side of the bed ($x = 0$) at the end of blowdown ($x = 0$) vs. number of cycles.

of cycles needed to reach the cyclic steady state varies from 6 to 40 in the isothermal case, increasing when the product cut decreases. The CPU time for one cycle at cyclic steady state is 10–15 s for different conditions. In the adiabatic case, hundreds of cycles are needed to reach the cyclic steady state due to difficulty in building up the temperature profile in the bed, as will be discussed in detail in the following section. The CPU time for one cycle at steady state is about 15–20 s.

Evolution from the different initial conditions

The evolution of several parameters of a PSA process from different initial conditions to the cyclic steady state has been studied by Rodrigues et al. (1992b). No multiple steady states, or quasi-steady states were found in the simulations. However, hundreds of cycles were needed to obtain the cyclic steady state for high product purity when the intraparticle mass-transfer resistance was taken into account. LeVan and Croft (1992) and Smith and Westerberg (1992) have developed methods to determine the adsorption cyclic steady state.

In this and following sections, fixed step times were used in the simulations, that is, $\theta_p = 2$, $\theta_f = 4$, $\theta_b = 10$, which means the cycle time is 7.5 s. Results reported here are based on 100 finite elements used in the bed to avoid numerical oscillations; 5 min

of CPU time for one cycle is needed. Results were printed using space intervals on the axial coordinate of 0.01. If intervals of 0.05 were used, no oscillations would have been seen, but shocks would not have been so nicely defined. Other parameters were: $k_o' = 2$, $q_o^* = 20$, $y_f = 0.5$, $y_o = 0$, 0.5, $\tilde{T}_o = \tilde{T}_f = 1$, $\Phi = 0.2$, $\beta_c = 1{,}537$, $u_o = 92$ cm/s, $u_r = 34.8$ cm/s, $P_e = 4.5$ bar, $\tau_o = 0.467$ s, which resulted in EN = 1.98, RE = 0.464, $N_{prod} = 0.295$ for the isothermal case, and EN = 1.863, RE = 0.549, $N_{prod} = 0.351$ for the adiabatic case.

The process parameters are enrichment (EN), recovery (RE), mole fraction (at $x = 1$) of the adsorbable species at the end of the feed step (y_{fe}), productivity (N_{prod}), and the temperatures at the end of the feed step (at $x = 1$) and at the end of the blowdown step (at $x = 0$), as a function of number of cycles for condition $y_o = 0$ (dashed lines) and $y_o = 0.5$ (full lines) in the isothermal and adiabatic cases are shown in Figures 7a-7e, respectively. From the figures, we can see that each process parameter for the equilibrium model using the different initial conditions goes to the same value at the cyclic steady state both in the isothermal and adiabatic cases, respectively. The effect of the initial condition on the evolution of the process parameters for various operating conditions was also checked. At cyclic steady state the mole fraction and the temperature axial profiles are exactly recovered whatever initial condition is used.

Comparing the evolution of the process parameters in the isothermal and in the adiabatic cases under the same operation conditions for $y_o = 0.5$ (Figure 7), we can find that less than 35 cycles are needed to reach the cyclic steady-state operation for the isothermal PSA; however, more than 200 cycles are needed for the adiabatic PSA. The enrichment of the light species is higher, but the recovery of the light species and the adsorbent productivity are lower in the isothermal case than in the adiabatic cases under the same operating conditions. This is because the temperature variation in the adsorption bed decreases the adsorption capacity of the adsorbent, which leads to a deeper penetrated mole fraction front of the adsorbable species in the bed in adsorption steps and less pressurization and blowdown amounts in the pressurization and blowdown steps (Lu et al., 1992). In the feed step, the temperature variation gives a higher product amount since less adsorbable species is adsorbed; in fact, we used fixed mole flux at the feed side of the bed and fixed feed step time. So, finally we get better enrichment, but worse recovery and productivity in comparing the isothermal and adiabatic adsorption beds under the same operating conditions. However, it should be kept in mind that the temperature variation in an adsorption bed always causes worse effects in the separation performance. If we compare the isothermal and adiabatic cases for the same enrichment of the light species, as shown in the Figure 6, we will get higher recovery and so higher productivity in the isothermal case. This is similar to what we have discussed before (Rodrigues et al., 1992b) when comparing the equilibrium and the intraparticle diffusion models.

It should be noted that in the simulations of the adiabatic adsorption bed, the changes of the process parameters from cycle to cycle are very small, sometimes less than 0.1%; however, this does not mean that the cyclic steady state is reached. The selection of the criteria to know if the cyclic steady state is reached should be based on the bed dynamics discussed in the following section.

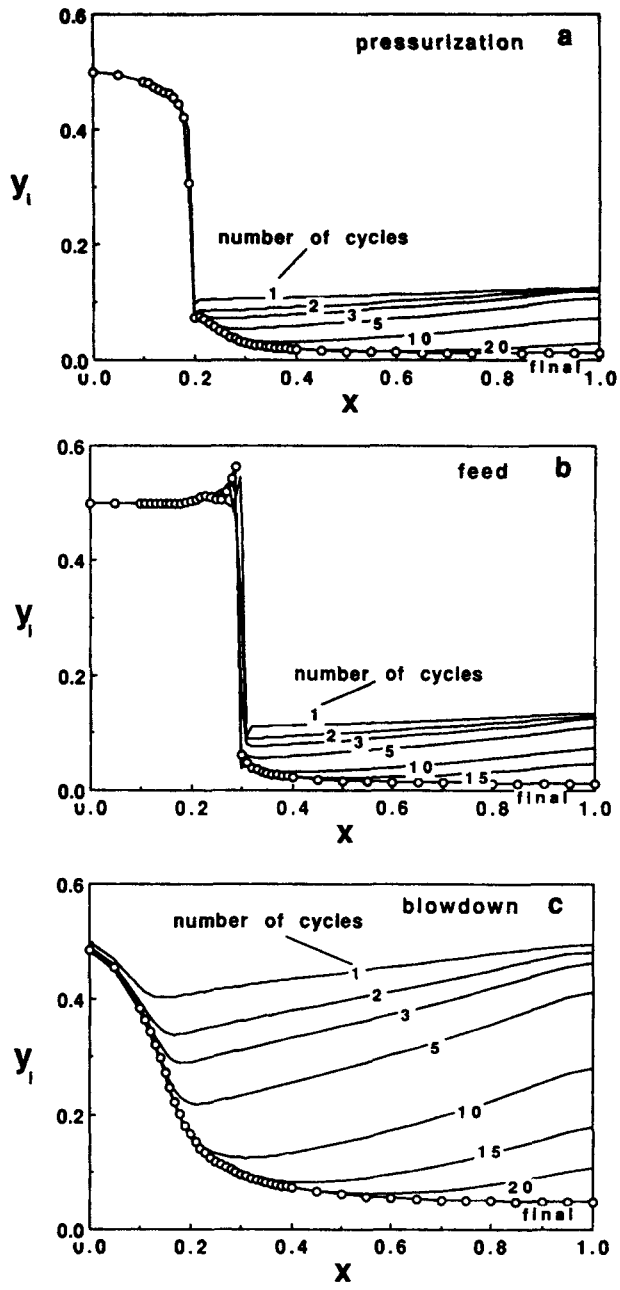

Figure 8. Axial mole fraction profiles y_i of the adsorbable species inside the bed at the ends of pressurization (a), feed (b) and blowdown (c) during evolution from the initial condition ($y_o = 0.5$) to the cyclic steady state in the isothermal case.

The development of axial mole fraction profiles of the adsorbable species at the end of pressurization, feed and blowdown steps from a uniform initial mole fraction in the bed ($y_o = 0.5$) to the cyclic steady state in the isothermal case is shown in Figures 8a-8c, respectively. The values of the mole fraction inside the bed gradually approach the values at the cyclic steady state from cycle to cycle, and they do not change much in the part of the bed near the feed side. The development of the mole fraction profile occurs mainly in the part of the bed near the production side. Numerical oscillation was found

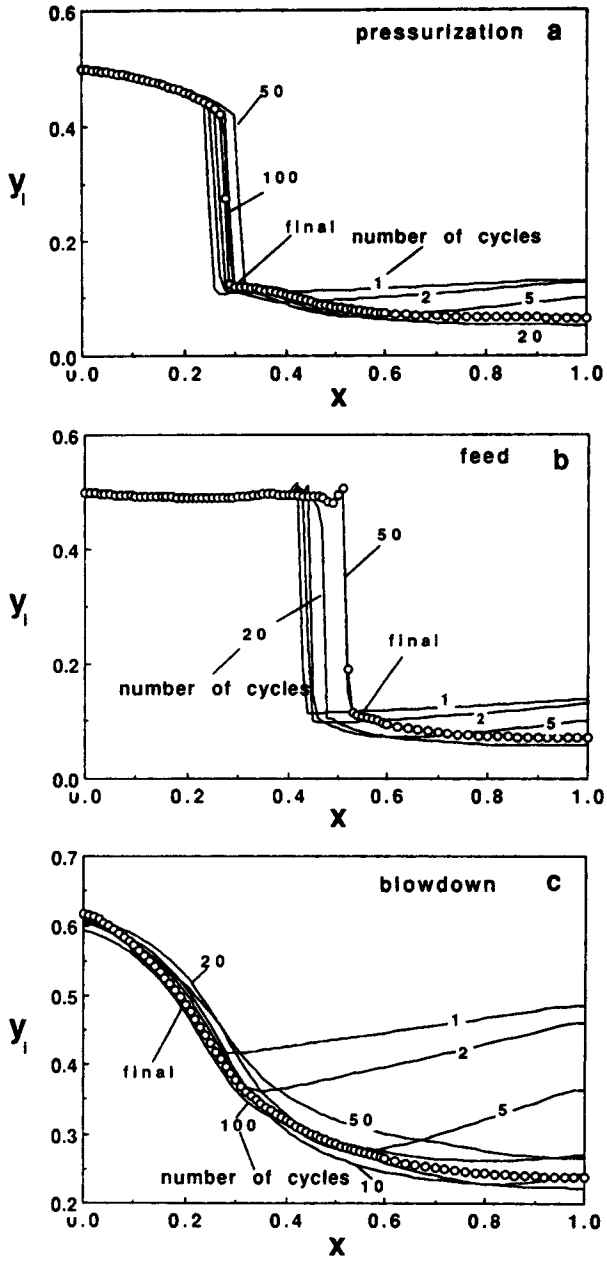

Figure 9. Axial mole fraction profiles y_i of the adsorbable species inside the bed at the ends of pressurization (a), feed (b) and blowdown (c) during evolution from the initial condition ($y_o = 0.5$) to the cyclic steady state in the adiabatic case.

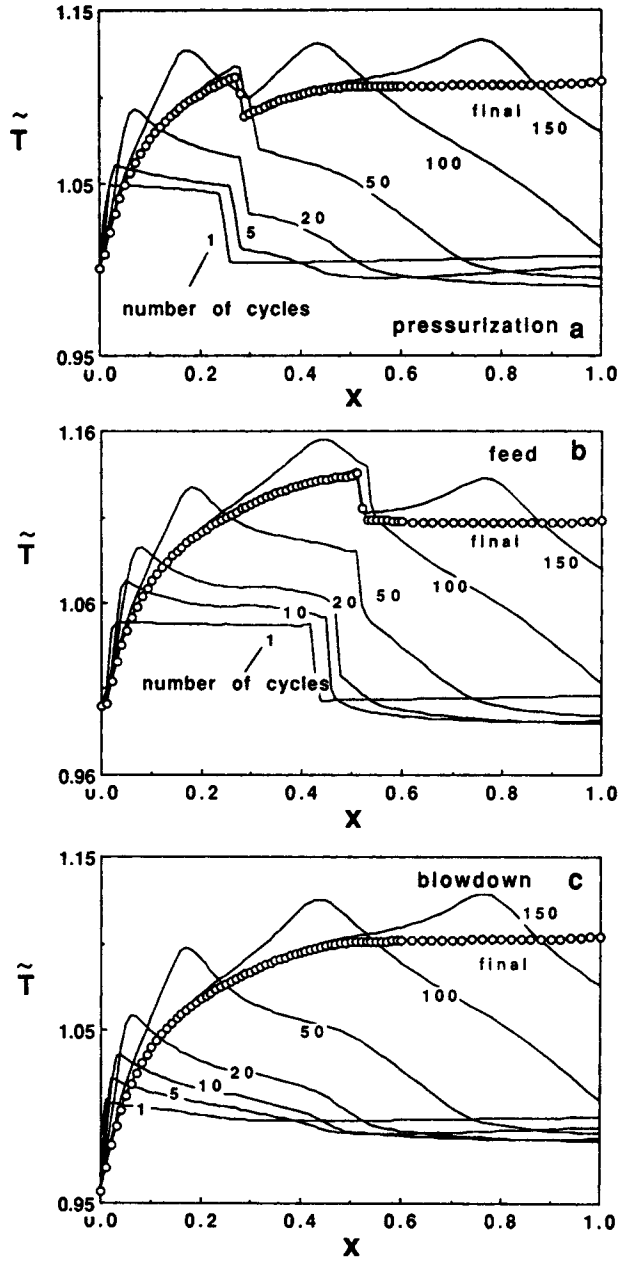

Figure 10. Axial reduced temperature profiles $\tilde{T}$ inside the bed at the end of pressurization (a), feed (b) and blowdown (c) during evolution from the initial condition ($y_o = 0.5$) to the cyclic steady state in the adiabatic case.

in the high mole fraction region due to the very high Peclet number in the model equation, as we have noticed before (Lu et al., 1992, 1993). However, we think that this does not affect the general process performance, because the numerical oscillation only appears in an unimportant region.

Figures 9a-9c and Figures 10a-10c show the evolution of axial mole fraction profiles and axial temperature profiles, respectively, in the adiabatic adsorption bed at the end of the three steps. The mole fraction front travels deeper inside the bed and the values of the mole fraction is higher in the downstream region in the adiabatic case when compared with the isothermal case. This is so because of the decrease of the adsorption capacity caused by the temperature variation. The values of temperature go through extreme values except at $x = 0$, and they pass through minimum and maximum values in the downstream region of the mole fraction front, which can also be seen in Figures 7e and 10. An interesting point shown in Figure 10, is that many cycles are needed to build up the temperature plateau at the production side of the bed. At the feed side of the bed, the temperature changes between the feed fluid temperature $\tilde{T}_f$ (in pressurization and feed steps)

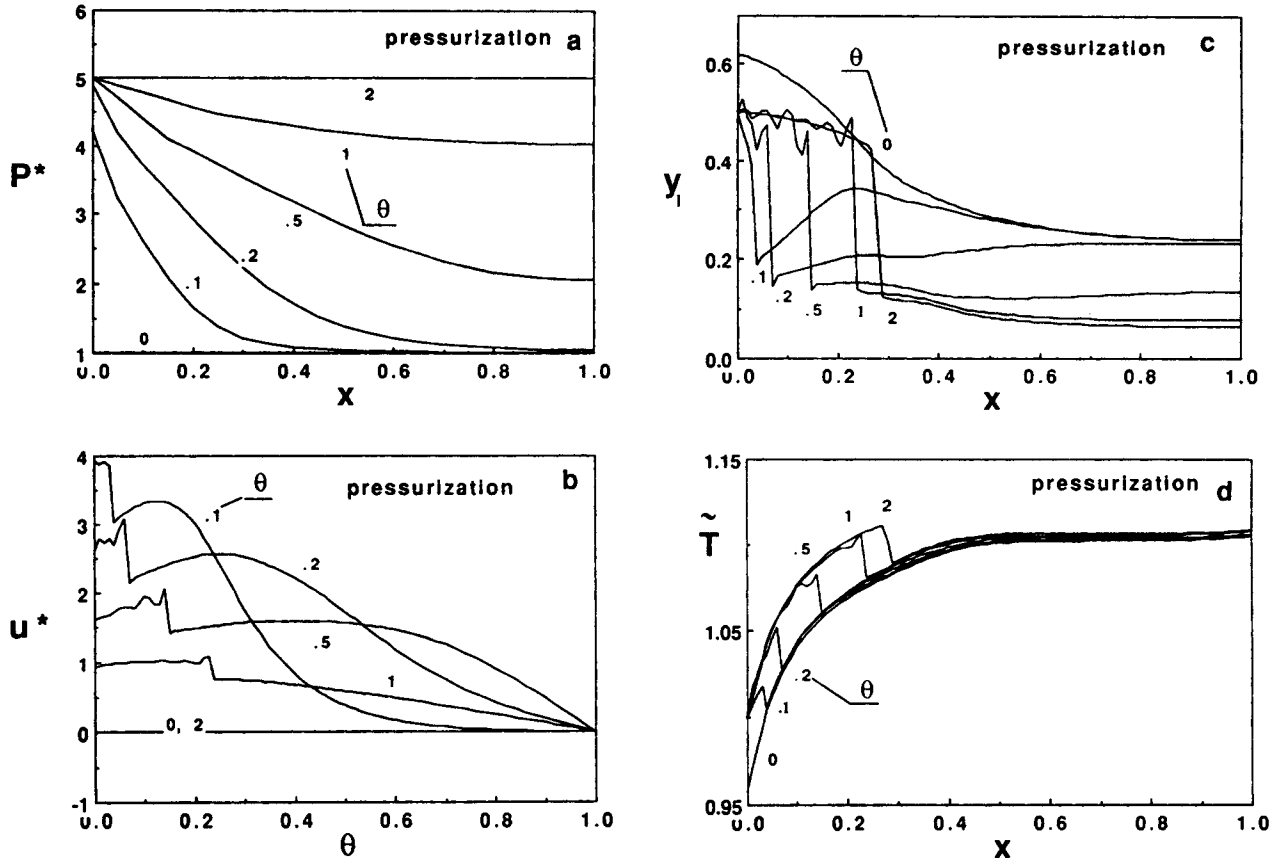

Figure 11. Axial profiles of reduced pressure P^* (a), reduced velocity u^* (b), mole fraction y_i (c) and reduced temperature $\tilde{T}$ (d) at different times during pressurization under cyclic steady state in the adiabatic case.

and the temperature plateau found in blowdown (Lu et al, 1992), and the latter is lower than $\tilde{T}_f$ and it is quickly reached (Figure 10c). At the production side of the bed, there is another temperature plateau in this three step one column PSA process which follows the global thermal balance at the cyclic steady state. It is expected that higher axial effective thermal conductivity reduces the time to reach the cyclic steady state.

Bed dynamics at cyclic steady state

The bed dynamics have been studied in the individual pressurization and blowdown steps in the isothermal and the adiabatic cases (Lu et al., 1992, 1993). However, the initial conditions in the bed were given arbitrarily, and they usually are different from the cyclic steady-state operation. Here, we follow the adiabatic adsorption bed treated in the above section and discuss the bed dynamics in the three steps under the cyclic steady-state operation.

Pressurization. The axial profiles of reduced pressure P^*, reduced velocity u^*, mole fraction y_i and reduced temperature at different times during pressurization in the adiabatic case are shown in Figures 11a–11d, respectively. The behavior of the first two parameters (P^* and u^*) is very similar to that we found before, when dealing with the pressurization step only (Lu et al., 1992), although the initial mole fraction and temperature profiles in the bed are very different. The shock wave in the mole fraction profiles and increased temperature wave coinciding with the mole fraction wave in Figure 11c and 11d can be observed; however, temperature profiles in the downstream region are almost flat and change very little. This is because the nonuniform temperature profile initially exists inside the bed and increases with the space distance as shown in Figure 11d; so, the colder fluid is pushed to the closed end of the bed during pressurization; the adsorption capacity has been reduced by more than a factor of two, that is, $q^* < 10$, due to the existence of the high temperature plateau $\tilde{T} = 1.105$ in that region.

Feed. The feed step is very similar to the normal adsorption bed operation. The results reported in Figures 12a–12d were based on constant pressure P_e at the production end of the bed and constant mole flux $u_r P_h$ at the feed end of the bed. At very short time, higher velocity was observed at the production end of the bed. After short time development, two velocity plateaus before and after the mole fraction front of the adsorbable species can be seen in Figure 12b. The former one is higher than the latter one, corresponding to different pressure drops in these regions. The front of the mole fraction of the adsorbable species becomes more and more steep due to the favorable nature of the adsorption isotherm. The temperature wave front still travels with the mole fraction wave front. Except in the region where adsorption occurs, the temperature and mole fraction inside the bed almost do not change.

Blowdown. The behavior of axial profiles of reduced pres-

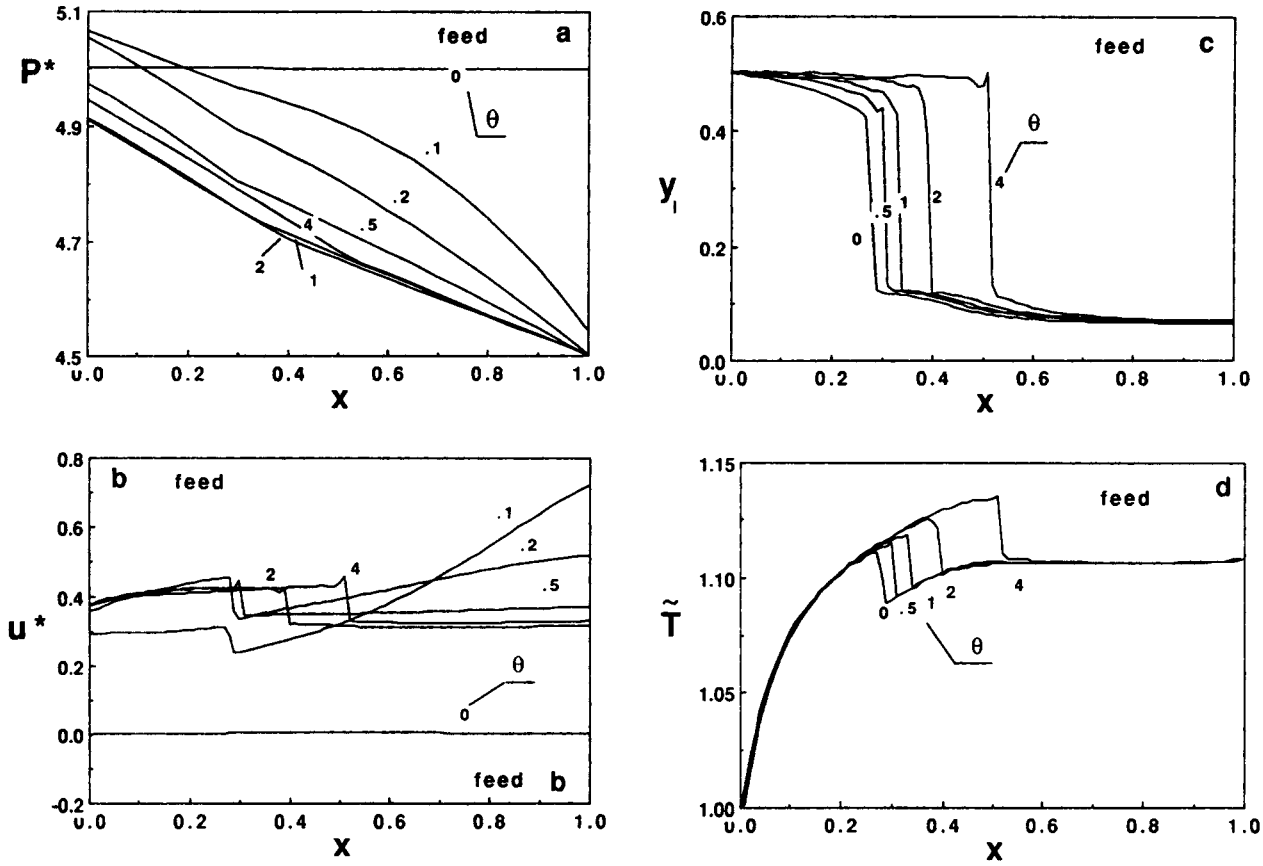

Figure 12. Axial profiles of reduced pressure P^* (a), reduced velocity u^* (b), mole fraction y_i (c) and reduced temperature $\tilde{T}$ (d) at different times during feed under cyclic steady state in the adiabatic case.

sure and velocity during blowdown, as shown in Figures 13a,b, are also similar to that observed in the study of the individual step (Lu et al., 1992). The two mole fraction plateaus and one temperature plateau at the open end of the bed can still be found during blowdown although the mole fraction and temperature inside the bed are nonuniform initially. In the downstream region of the mole fraction front, the mole fraction and the temperature profiles are always flat, and the temperature changes very little. The reason is the same as that we pointed out in pressurization, that is, the very small adsorption capacity caused by the high temperature in that region.

Histories of the reduced pressure P^*, reduced velocity u^*, mole fraction y_i and reduced temperature $\tilde{T}$ at four spacial positions, $x=0$, 0.1, 0.5, 1, in one cycle under cyclic steady state are shown in Figures 14a–14d, respectively. The behavior shown in these figures is not changed much from that of individual step studies (Lu et al., 1992). From the study of bed dynamics under cyclic steady-state operation, it is interesting to try to make some simple analysis and predictions after we have learned about process behavior, such as to predict the plateaus of the mole fraction and temperature through some simplified mass and thermal balances as done before (Lu et al., 1992, 1993).

Conclusions

A mathematical model for pressure swing adsorption has been proposed in this article and used to analyze a simple cycle with complex dynamics for separation of a binary mixture of one inert and one adsorbable species in a three step, one column process. The model combines material, energy and momentum balances with a nonlinear isotherm to study the behavior of a bed with unpacked regions at its ends for different parameters and operating conditions. Three specific problems have been considered: (i) performance under various operating conditions; (ii) evolution of the process from different initial conditions; and (iii) bed dynamics at the cyclic steady state.

In a parametric study of performance under various operating conditions, we considered isothermal and adiabatic operation, isotherm effects, incomplete pressurization and blowdown, and the influence of dead volumes at the ends of the column. Process performance was characterized by enrichment, productivity and recovery. The enrichment-cut relation predicted by the equilibrium model in isothermal and adiabatic cases is linear, and so the enrichment-recovery curve has a concave shape. The separation performance of the process almost does not change with the nature of adsorption isotherm, but it strongly depends on the adsorption capacity of adsorbent. Except for a small product cut, that is, small recovery of the inert species, incomplete pressurization does not affect the enrichment-recovery relation much; however, incomplete blowdown obviously decreases it, and so a somewhat longer exhaust step is suggested. Small improvement on the separation performance of the process by the bottom "dead volume" was found at high recovery of the inert species; however, the separation performance decreases when the top "dead volume" increases for a given recovery.

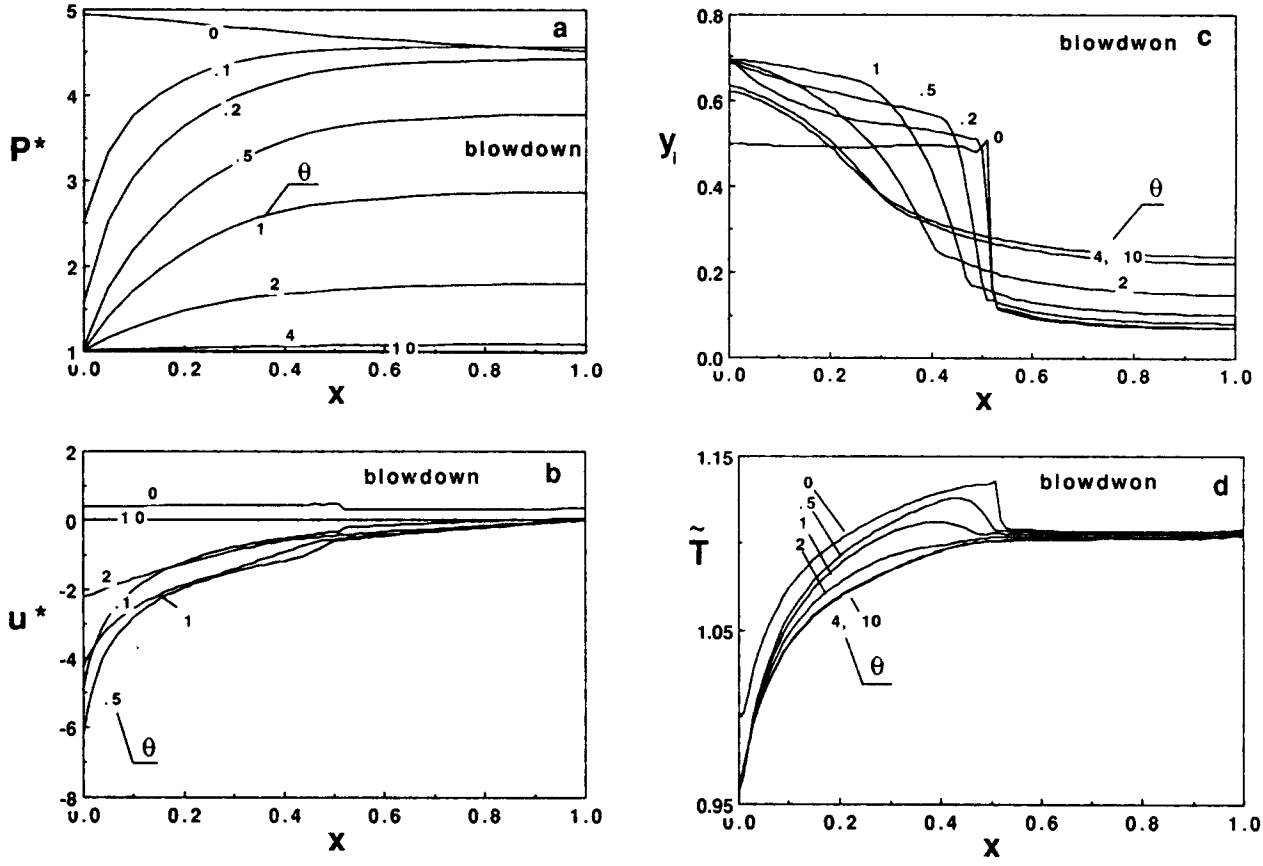

Figure 13. Axial profiles of reduced pressure P^* (a), reduced velocity u^* (b), mole fraction y_i (c) and reduced temperature $\tilde{T}$ (d) at different times during blowdown under cyclic steady state in the adiabatic case.

The evolution of the process from the different initial condition to the cyclic steady state in isothermal and adiabatic cases was addressed by focusing on the changes of several process parameters and the development of axial mole fraction and temperature profiles from cycle to cycle; no multiple cyclic steady states were found. The cyclic steady state for the isothermal case is easily reached; however, hundreds of cycles are needed to reach the cyclic steady state in the adiabatic case due to the difficulty of building up the temperature profile in the bed. Very small changes in the process profiles with each cycle in that case do not mean that the cyclic steady state has been reached.

The bed dynamics at the cyclic steady state have been studied in the three individual steps (pressurization, feed and blowdown) by looking at the axial profiles and histories of the process parameters at four positions inside the bed. A temperature plateau in the part of the bed near the production side was found and it does not change much during operation. The mole fraction downstream of the mole fraction front in the bed is almost always flat from step to step. Finally, two velocity plateaus before and after the mole fraction front of the adsorbable species were observed in the feed step.

Acknowledgments

Financial support from FUNDAÇÃO ORIENTE, JNICT, NATO CRG 890600 and EEC JOULE 0052 is gratefully acknowledged.

Notation

$b_1, \ldots, b_4$ = dimensionless constants
BE = pressure criterion for blowdown
c = total concentration in the bulk fluid phase, mol/cm^3
c_h = the concentration at the high pressure, mol/cm^3
c_o = total concentration in the bulk fluid phase under the reference condition, mol/cm^3
c_{pg} = heat capacity of gas at constant pressure, cal/mol·K
c_{ps} = heat capacity of solid, cal/g·K
c_{vg} = heat capacity of gas at constant volume, cal/mol·K
CUT = product cut, stated by Eq. 32
d_p = adsorbent particle diameter, cm
D = bed diameter, cm
D_{ax} = axial mass dispersion coefficient, cm^2/s
D_{mo} = molecular diffusivity at reference conditions, cm^2/s
EN = enrichment of the light species, stated by Eq. 28
f = dimensionless total concentration in the bulk fluid phase
f_e = dimensionless total concentration at the production end
f_h = dimensionless high total concentration
f_l = dimensionless low total concentration
h_w = heat-transfer coefficient between the bulk fluid and the column wall, cal/cm^2·s·K
$-\Delta H$ = heat of adsorption, cal/gmol
k = parameter of the Langmuir equilibrium relation, cm^3/mol
k' = constant for the normalized equilibrium relation, Eq. 7
k_{hg} = thermal conductivity of gas, cal/cm·s·K
k_{hx} = effective axial heat conductivity, cal/cm·s·K

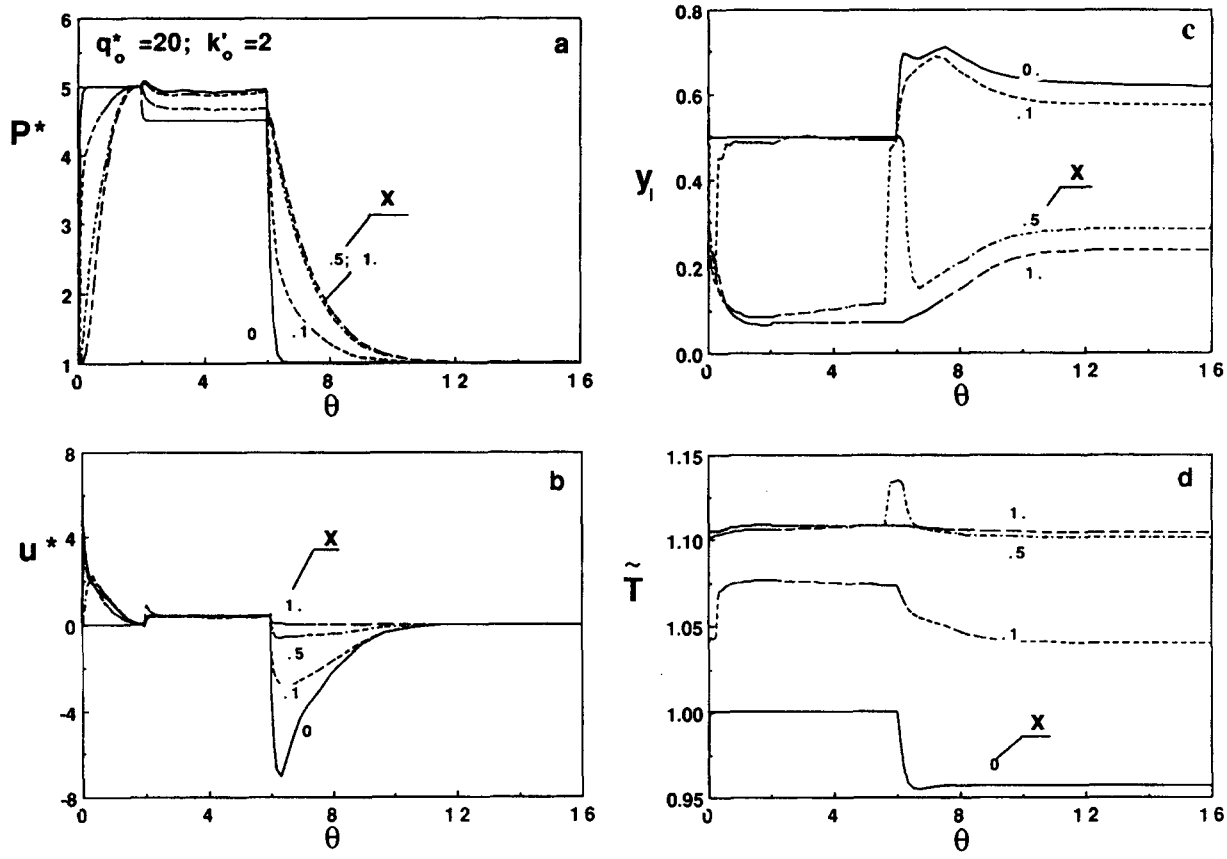

Figure 14. Histories of reduced pressure P^* (a), reduced velocity u^* (b), mole fraction y_i (c) and reduced temperature $\tilde{T}$ (d) at different space positions in one complete cycle under cyclic steady state in the adiabatic case.

k_o' = reference constant for the normalized equilibrium relation, Eq. 10
k_o = parameter of the Langmuir equilibrium relation at reference temperature, cm^3/mol
L = bed length, cm
M_p, M_b = pressurization and blowdown rate parameters
N_f, N_p = dimensionless pressurization and feed rate, stated by Eq. 33
N_{prod} = dimensionless productivity, stated by Eq. 30
P = pressure in the bulk fluid, Pa
P^* = dimensionless pressure in the bulk fluid
P_e = production side pressure, Pa
P_e^* = dimensionless production side pressure
P_h = high pressure, Pa
P_h^* = dimensionless high pressure
P_l = low pressure, Pa
P_l^* = dimensionless low pressure
P_o = atmospheric pressure, Pa
Pe_h = heat Peclet number in the bulk fluid
Pe_m = mass Peclet number in the bulk fluid
PE = pressure criterion for pressurization
q^* = constant for the normalized equilibrium relation, Eq. 7
q_m = parameter of the Langmuir equilibrium relation, mol/cm^3
q_o^* = reference constant for the normalized equilibrium relation, Eq. 10
R = ideal gas constant (= 1.987 cal/mol·K)
RE = recovery of the light species, stated by Eq. 31
t = time, s
T = temperature in the bulk fluid, K
$\tilde{T}$ = reduced temperature in the bulk fluid
$\tilde{T}_f$ = reduced feed temperature
T_{oo} = reference temperature (= 298 K), K
$\tilde{T}_o$ = reduced initial temperature in the bed
$\tilde{T}_w$ = reduced temperature at the column wall
u = superficial velocity in the bulk fluid, cm/s
u^* = dimensionless velocity in the bulk fluid
u_o = superficial velocity under the reference conditions, cm/s
u_p^* = dimension pressurization velocity
u_r^* = dimension feed velocity
x = dimensionless axial coordinate in the bed
y_B = mole fraction of the adsorbable species in the bottom "dead volume"
y_f = mole fraction of the adsorbable species in the feed
y_{fe} = mole fraction of the adsorbable species for the production end of the bed at the end of feed step
y_i = mole fraction of the adsorbable species in the bed
y_o = initial mole fraction in the bed
$\bar{y}_p$ = average mole fraction of the adsorbable species in the product

Greek letters

α_{hw} = ratio between the time constant for column wall heat transfer and the reference space time
β_T, β_B = volume parameter of the top and bottom "dead volume"
$\beta_h, \beta_r, \beta_c$ = dimensionless constants defined by Eq. 8
γ_1, γ_2 = parameters
γ_1', γ_2' = parameters
ϵ = bed porosity
ϵ_p = adsorbent porosity
θ = time reduced by the reference space time

$\theta_t, \theta_p, \theta_f, \theta_b$ = dimensionless cycle, pressurization, feed and blowdown times
μ = fluid viscosity, g/cm s
ρ_o = fluid density, g/cm^3
ρ_s = partical density, g/cm^3
Φ = concentration ratio (c_o/c_h)

Literature Cited

Cen, P. and R. T. Yang, "Bulk Gas Separation by Pressure Swing Adsorption," *Ind. Eng. Chem. Fundam.*, **25**, 758 (1986).

Cheng, H. C., and F. B. Hill, "Separation of Helium-Methane Mixtures by Pressure Swing Adsorption," *AIChE J.*, **31**, 95 (1985).

Doong, S. J., and R. T. Yang, "The Role of Pressure Drop in Pressure Swing Adsorption," *AIChE Symp. Series*, **45**(84), 264 (1988).

Flores Fernandez, G., and C. N. Kenney, "Modeling of the Pressure Swing Air Separation Process," *Chem. Eng. Sci.*, **38**, 827 (1983).

Hart, J., M. Battrum, and W. J. Thomas, "Axial Pressure Gradients During Pressurization and Depressurization Steps of a PSA Gas Separation Cycle," *Gas Separation and Purification*, **4**, 97 (1990).

Jones, R. L., and G. E. Keller, "Pressure Swing Parametric Pumping—A New Adsorption Process," *J. Separ. Proc. Technol.*, **2**, 17 (1981).

Kayser, J. C., and K. S. Knaebel, "Pressure Swing Adsorption: Experimental Study of an Equilibrium Theory," *Chem. Eng. Sci.*, **41**, 2931 (1986).

Kayser, J. C., and K. S. Knaebel, "Pressure Swing Adsorption: Development of an Equilibrium Theory for Binary Gas Mixtures with Nonlinear Isotherms," *Chem. Eng. Sci.*, **44**, 1 (1989).

Knaebel, K. S., and F. B. Hill, "Pressure Swing Adsorption: Development of an Equilibrium Theory for Gas Separation," *Chem. Eng. Sci.*, **40**, 2351 (1985).

Kowler, D. E., and R. H. Kadlec, "The Optimal Control of a Periodic Adsorber," *AIChE J.*, **18**, 1207 (1972).

Kumar, R. "Adsorption Column Blowdown: Adiabatic Equilibrium Model for Bulk Binary Gas Mixtures," *Ind. Eng. Chem. Res.*, **28**, 1677 (1989).

LeVan, M. D., and D. T. Croft, "Direct Determination and Multiplicity of Periodic States of Adsorption Cycles," presented at the Fourth International Conference on Fundamentals of Adsorption, Kyoto, Japan (May 1992).

Lu, Z. P., J. M. Loureiro, M. D. LeVan, and A. E. Rodrigues, "Pressurization of Adsorption Beds. II—Effect of the Momentum and Equilibrium Relations on the Isothermal Operation," accepted *Chem. Eng. Sci.*, **48**(9), 1699 (1993).

Lu, Z. P., J. M. Loureiro, M. D. LeVan, and A. E. Rodrigues, "Pressurization and Blowdown of an Adiabatic Adsorption Bed III," *Gas Sep & Purif.*, **6**, 15 (1992).

Ramkrishna, D., and N. R. Amundson, "Stirred Pots, Tubular Reactors, and Self-Adjoint Operators," *Chem. Eng. Sci.*, **29**, 1353 (1974).

Rodrigues, A. E., J. M. Loureiro, and M. D. LeVan, "Simulated Pressurization of Adsorption Beds," *Gas Separation and Purification*, **5**, 115 (1991a).

Rodrigues, A. E., Z. P. Lu, J. M. Loureiro, and M. D. LeVan, "Pressurization of Adsorption Beds," NSF-CNRS Workshop on Adsorption Processes for Gas Separation, Gif-sur-Yvette, France (1991b).

Rodrigues, A. E., Z. P. Lu, J. M. Loureiro, and M. D. LeVan, "Diffusion and Convection in Pressure Swing Adsorption Processes," presented at the Fourth International Conference on Fundamentals of Adsorption, Kyoto, Japan (May 1992a).

Rodrigues, A. E., Z. P. Lu, and M. D. LeVan, "Effect of the Intraparticle Convection on a Cycle of Three-Step One-Column Pressure Swing Adsorption Process," presented at the AIChE Meeting, Miami Beach (Nov. 1992b).

Ruthven, D. M. *Principles of Adsorption and Adsorption Process*, Wiley, New York (1984).

Scott, D. M. "Similarity Solutions for Pressurization and Depressurization with a Two-Component Gas in an Adsorbing Bed," *Chem. Eng. Sci.*, **46**, 2977 (1991).

Smith IV, O. J., and A. W. Westerberg, "Acceleration of Cyclic Steady State Convergence for Pressure Swing Adsorption Models," *Ind. Eng. Chem. Res.*, **31**, 1569 (1992).

Shu, S. S., and P. C. Wankat, "Pressure Swing Adsorption for Binary Gas Separation with Langmuir Isotherms," *Chem. Eng. Sci.*, **44**, 2406 (1989).

Suh, S. S., and P. C. Wankat, "Combined Cocurrent-Countercurrent Blowdown Cycle in Pressure Swing Adsorption," *AIChE J.*, **35**, 523 (1989).

Sundaram, N., and P. Wankat, "Pressure Drop Effects in the Pressurization and Blowdown Steps of Pressure Swing Adsorption," *Chem. Eng. Sci.*, **43**, 123 (1988).

Turnock, P. H., and R. H. Kadlec, "Separation of Nitrogen and Methane via Periodic Adsorption," *AIChE J.*, **17**, 335 (1971).

Wakao, N., and B. H. Chen, "Some Models for Unsteady-State Heat Transfer in Packed Bed Reactors," *Recent Treads in Chemical Reaction Engineering*, pp. 254, Vol. 1, B. Kulkarni, R. Mashelkar and M. Sharma, eds., Wiley Eastern Ltd., New Delhi (1987).

Yang, R. T., *Gas Separation by Adsorption Processes*, Butterworths, Boston (1987).

Yang, R. T., and P. L. Cen, "Improved Separation by Pressure Swing Adsorption Processes for Gas Separation: By Heat Exchange between Adsorbers and by High-Heat-Capacity Inert Additives," *Ind. Eng. Chem. Des. Dev.*, **25**, 54 (1986).

Manuscript received Oct. 6, 1992, and revision received Feb. 8, 1993.